Dynamics and thermodynamics of supercooled liquids and glasses from a model energy landscape

David J. Wales and Jonathan P. K. Doye
University Chemical Laboratories, Lensfield Road, Cambridge CB2 1EW, United Kingdom
(Received 24 October 2000; published 16 May 2001)

The dynamics and thermodynamics of a model potential-energy surface are analyzed with regard to supercooling and glass formation. Relaxation is assumed to be mediated by pathways that connect groups of local minima. The dynamics between these groups is treated via transition state theory using appropriate densities of states consistent with the thermodynamics of the model, with a general expression for the free energy barrier. Nonergodicity is admitted by successive disconnection of regions that no longer contribute to the partition function as a function of the observation time scale. The model exhibits properties typical of supercooled liquids and glasses spanning the whole range of ''fragile'' and ''strong'' behavior. Non-Arrhenius dynamics, characteristic of ''fragile'' glass formers, are observed when the barriers to relaxation increase as the potential energy decreases, but only if the observation time scale is long enough. For a fixed observation time, fragility generally increases as the free energy barriers decrease and vibrational frequencies increase. We associate higher vibrational frequencies with systems that have more local minima, and hence when the model exhibits dynamic fragility we usually see a large change in the heat capacity at the glass transition. However, in some regions of parameter space the expected correlations between dynamics and thermodynamics are not present.

DOI: 10.1103/PhysRevB.63.214204 PACS number(s): 64.70.Pf, 82.20.Wt, 82.20.Kh, 64.60.My

I. INTRODUCTION

Within the Born-Oppenheimer approximation, the structure, dynamics, and thermodynamics of any given system are determined by the underlying potential-energy surface (PES) or potential energy ''landscape.'' However, if the temperature is not too low the hydrodynamically based mode-coupling theory[1–3] (MCT) can provide a satisfactory account of the relaxation behavior in many glass formers. Here we focus upon the ''activated'' regime, where potential and free energy barriers significant compared to kT must be overcome. The present PES-based approach should work for higher temperatures too, until the system ceases to spend sufficient time in each minimum to establish equilibrium properties.[4]

The most important features of the PES are stationary points where the force vanishes. In particular, a local minimum (or ''inherent structure'' [5]) is a stationary point with no negative force constants (imaginary normal mode frequencies) whilst a true transition state has precisely one. The number of stationary points probably grows exponentially with the size of the system.[6–8] Nevertheless, over the last decade significant progress has been made in characterizing the global PES's of increasingly complex systems.[4,9–34] Some of the ideas have developed in parallel for finite systems, glasses and proteins, and it is from the latter biological viewpoint that the concept of a free-energy folding funnel originates.[13,35–39] Studies of model *free* energy landscapes for proteins[40–44] complement the present analysis of global *potential* energy surfaces.

Goldstein made an important contribution when he proposed a connection between the properties of glasses and the PES.[45] He distinguished two time scales: rapid vibrations about local minima and less frequent jumps over significant energy barriers. Johari and Goldstein subsequently observed two different characteristic relaxation times in dielectric loss spectra, naming the slower one α and the other one β, and they associated the α relaxation peak with slower rearrangement mechanisms of some sort.[46]

Adam and Gibbs,[47] building upon the model of Gibbs and DiMarzio,[48] made a heuristic connection between dynamics and thermodynamics by assuming that relaxation occurs via ''cooperatively rearranging regions'' whose size increases with decreasing temperature. However, modifications are needed to fit experimental data,[49] and recent results for metallic glass formers suggest that two distinct sorts of mechanisms contribute to transport processes.[50] On the other hand, several recent simulation studies support the original formulation.[51–53] Xia and Wolynes have recently exploited the near universality of the Lindemann ratio to provide an alternative connection based upon density functional theory.[54] In the present study we solve a model that is based on general properties of global potential-energy surfaces without reference to the details of the potential or to the particular relaxation mechanisms. This model, which attempts to reconcile nonergodic dynamics and thermodynamics in a consistent framework, is described in Sec. II. Some characteristic properties of the model are discussed in Sec. III, and numerical results are presented in Sec. IV. Conclusions follow in Sec. V.

II. THE MODEL

The present model is in some ways an extension of our previous analysis that focused on relaxation to the global potential-energy minimum.[13] Here we distinguish between rearrangements that facilitate further relaxation to lower potential-energy regions of the PES from rearrangements within given sets of local minima that span a limited range of potential energy.

Master equation dynamics based on a biased random walk[55] have previously reproduced the multiexponential relaxation observed for the binding kinetics of carbon monoxide to heme proteins.[56] Brawer's kinetic model views diffu-

sion as the cooperative motion of a number of atoms via high-energy transition states,[57] but the results assume that these ''transition states'' are equally accessible from any higher density structure. In the present model no assumptions are required about the nature of the rearrangements since we focus on the role of a given PES. However, the division of the system into regions corresponding to subsets of atoms is common to a number of earlier theories,[47,58–60] and more recently to the frustration-limited domain model.[61]

Dyre recast Brawer's model as an energy master equation.[62] However, this formulation does not appear to admit the connectivity of the PES: at least one further order parameter is needed to distinguish states of the same energy that belong to different regions, otherwise there can be no barrier between them. This minimal two-order parameter picture, using energy and regions, is different, but probably not incompatible, with that of Tanaka, who has suggested that competition between density ordering and bond ordering can provide a universal description of the glass transition.[63,64]

Bässler's explanation for non-Arrhenius dynamics,[65] in terms of a decreasing mean energy that leads to an increasing mean activation energy with temperature, captures the same basic physics as the present model. A more elaborate energy master equation study, based upon structural changes on different energy scales, was used to distinguish strong and fragile glass formers,[66] but again assumes global connectivity. It is this feature of the model that probably leads to some of the undesirable behavior noted by Dyre.[67] Diezemann and coworkers have considered a locally connected version of the model[68–70] where transitions are only allowed between states that are sufficiently close in energy; however, there is again no concept of connectivity in configuration space.[71] Analytical solutions exist for globally connected master equations,[40,72] but unfortunately disappear when nontrivial connectivity is introduced.

An illustration of the model PES considered in the present work is shown in Fig. 1. The lowest energy region corresponds to the crystal and also contains local minima with predominantly crystalline order. These minima span the energy range $E_x \pm \delta/N$ per atom, so the region has depth 2δ. The remaining minima, which contribute to the liquid or glass configuration space, are divided into $N+1$ sets, according to their potential energy. Set a contains the minima with energies in the range $E_a \pm \delta$, where $E_a = -N\delta + 2(a-1)\delta$, and $a = 1,2,...,N+1$. The energy difference between adjacent sets is therefore 2δ, independent of N. A discrete number of regions rather than a continuous distribution is used to obtain a more convenient formulation of the global dynamics.

Often, it is useful to be able to look at the thermodynamic properties of certain selected regions of configuration space by restricting the integral in the partition function. In the current model we formulate a nonergodic canonical partition function, $Z(T,\tau)$, which depends on the time scale of observation, τ. $Z(T,\tau)$ is the sum of the partition functions for the crystalline (x) and noncrystalline (nx) regions, weighted by step functions to exclude those regions that are disconnected on the given time scale:

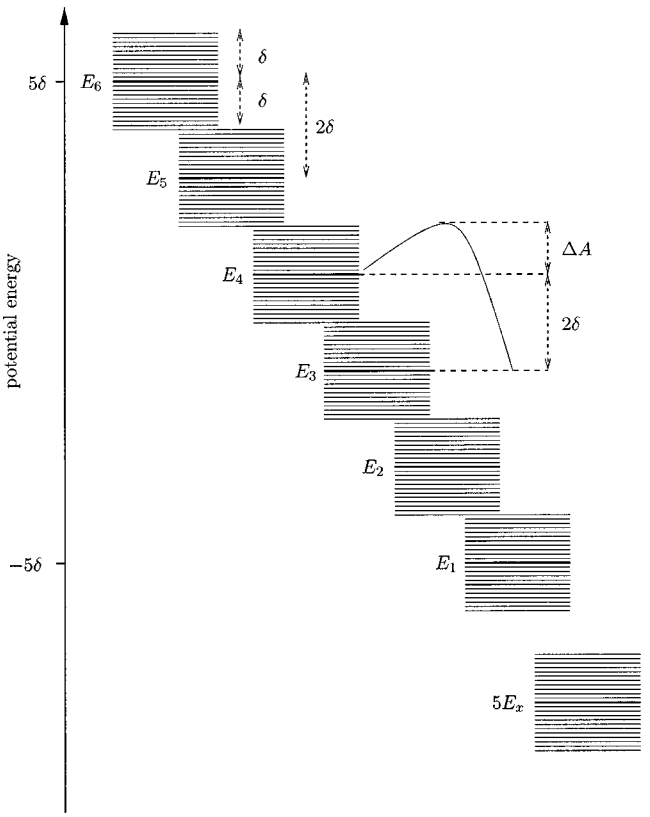

FIG. 1. A schematic depiction of the model potential-energy surface for $N=5$. The distribution of minima in each region is represented by a set of horizontal lines, and the uphill and downhill barriers are marked between regions 3 and 4.

$$Z(T,\tau) = Z_x(T)\Theta[f_x(T) - 1/\tau] + \sum_{a=1}^{N+1} Z_a(T)\Theta[f_a(T) - 1/\tau], \tag{1}$$

where Θ is the Heaviside step function and $f_a(T)$ is the probability flux out of region a at temperature T. In fact, f_a is also a function of τ because the flux depends upon which regions are connected. For each T and τ the nonergodic partition function, $Z(T,\tau)$, is calculated iteratively by removing disconnected regions and recalculating the fluxes until self-consistency is achieved. Thermodynamic properties are then obtained on the assumption of equilibrium between the remaining connected regions with renormalized occupation probabilities,

$$P_a(T,\tau) = Z_a(T)/Z(T,\tau). \tag{2}$$

The necessity to include such ergodicity breaking in both structural and spin glasses[73–76] is well known,[77,78] and the importance of the observation time scale has been discussed by Palmer[71] and Ma.[79]

The formulation leading to the partition function in equation (1) is an example of a restricted ensemble,[71] and is best regarded as a postulate. In Palmer's nomenclature[71] the regions are the smallest ''components'' considered in the present model, since we do not treat the individual local minima explicitly but subsume their contribution into the

regional partition function $Z_a(T)$ (Sec. II A). Properties of the model are calculated using the restricted partition function $Z(T,\tau)$, which should correspond to an individual experimental measurement. The appropriate $Z(T,\tau)$ is determined using a stochastic dynamical approach (Sec. II B).

It is important to note that the present ''regions'' of configuration space do not involve a restriction of the coordinates to a subset of atoms. The model therefore makes no assumptions about the existence of ''cooperative rearrangements'' in subclusters, for example. The issue of how the given PES arises from the detailed interatomic potential has been separated from the question of how the PES determines the thermodynamic and dynamical properties.

For a given τ we start from a high temperature $T_{\max}$ and calculate the required thermodynamic and dynamic properties at progressively lower temperatures, $T_{\max}-\delta T$, $T_{\max}-2\delta T$, etc. $Z(T,\tau)$ is computed iteratively at each point, with the proviso that regions above the highest-energy-connected region at the previous temperature cannot be reconnected. This rule expresses our intuition that probability density should not be able to climb back up the PES to regions that were frozen out at a higher temperature.

Freezing to a particular region occurs either when less than two regions remain kinetically connected, or stochastically when a region is disconnected that is associated with sufficient probability. Specifically, the occupation probability, $P_a(T+\delta T,\tau)$, of a region a that is disconnected at temperature T but connected at the previous temperature $T+\delta T$, is compared with a random number sampled from [0, 1]. Freezing is deemed to occur to region a if $P_a(T+\delta T,\tau)>0.5$ and exceeds the random number, otherwise the region is simply disconnected and the iterative calculation of $Z(T,\tau)$ continues. Further relaxation and loss of configurational entropy within each region is described by the model partition function $Z_a^{\mathbf{r}}(T)$ defined in Sec. II A. The temperature at which freezing to a single region occurs can be used as a definition of T_g, and T_g increases as the observation time scale decreases, as expected.[80] After freezing the total partition function simply becomes that of the region in question, $Z(T,\tau)=Z_a(T)$. Freezing to the crystal is certain to occur if it is connected at $T_m-\delta T$, since below the melting point T_m, the occupation probability of the crystal is almost unity if it is accessible. With a suitable choice of parameters the model will freeze reliably to the crystal at $T_m-\delta T$, which can be made arbitrarily close to T_m. However, we will concentrate on parameters that render the system a good glass former, where freezing to the equilibrium global free-energy minimum does not occur on the time scales of interest. Crystallization is avoided by choosing parameters that decrease the probability flux between the crystalline and noncrystalline regions. For example, lowering E_x or decreasing δ inhibits crystallization. In terms of the nucleation and growth view of this first-order phase transition, reliable glass formation is ensured when minima that support critical nuclei are kinetically inaccessible.

The determination of freezing introduces a stochastic element into our calculations. In practice the system may freeze into a few different neighboring regions for different random number sequences. However, in the present model the properties of these regions are very similar, and so there is no need to average the calculated properties over different runs.

A. Thermodynamics

We must now specify the regional partition function Z_a. We consider a constant-volume supercell that is periodically repeated to produce the bulk material. The numerical results presented in Sec. IV are all for $N=400$, which is large enough to produce a sharp (but not quite discontinuous) first-order phase transition at T_m when crystallization actually occurs. It should always be possible to describe the system in this way so long as there are no diverging correlations. The results for $N=400$ are almost converged to the $N\to\infty$ limit within the present model.

For each region the partition function is taken to be

$$Z_a(T)=\sum_{i\in a} Z_i^{\mathrm{vib}}(T)e^{-E_i/kT} \tag{3}$$

$$\approx Z_a^{\mathrm{vib}}(T)e^{-(E_a-\delta)/kT}\sum_{i\in a}\exp\{-[E_i-(E_a-\delta)]/KT\}$$

$$=Z_a^{\mathrm{vib}}(T)e^{-(E_a-\delta)/kT}Z_a^{\mathbf{r}}(T). \tag{4}$$

The first line assumes the usual superposition approximation[4,81–86] for the densities of states of all the local minima i within region a. In the second line we assume for convenience that each local minimum in this region has the same vibrational partition function $Z_a^{\mathrm{vib}}(T)$. The third line defines the regional configurational partition function $Z_a^{\mathbf{r}}(T)$, relative to an energy origin at $E_a-\delta$, the bottom of region a. $Z_a^{\mathbf{r}}(T)$ depends upon the detailed distribution of local minima, and should also depend upon the time scale of observation. Here we adopt a simple ansatz for $Z_a^{\mathbf{r}}(T)$ that has the expected limits for $T\to 0$ and $T\to\infty$. We have found that partition sums corresponding to energy densities of local minima that increase exponentially or geometrically with energy from the ground state can be accurately fitted by

$$Z_a^{\mathbf{r}}(T)=\exp\left[\frac{N\sigma_a T}{T+T_{3/4}}\right], \tag{5}$$

which has limits

$$\lim_{T\to 0} Z_a^{\mathbf{r}}(T)=1 \quad \text{and} \quad \lim_{T\to\infty} Z_a^{\mathbf{r}}(T)=\exp(N\sigma_a). \tag{6}$$

For the crystalline region we take

$$Z_x^{\mathbf{r}}(T)=\exp\left[\frac{N\sigma_x T}{T+T_{3/4}}\right],$$

and for σ_a we assume

$$\sigma_a = \sigma_x + \sigma_{\rm shift} + \sigma_{nx}\left[1 - \left(\frac{E_a}{N\delta}\right)^2\right]. \quad (7)$$

At $T=0$ only the lowest energy minimum in the region contributes to $Z_a^{\mathbf{r}}$, while in the $T\to\infty$ limit $Z_a^{\mathbf{r}}$ is just the total number of minima in the region, $\exp(N\sigma_a)$. The empirically observed[87] and theoretically justified[6–8] exponential scaling of the number of minima with system size is therefore ensured. The entropy of a glass that solidifies from any region also tends smoothly to zero as $T\to 0$, as expected by other authors.[84,88] This limit is further discussed in Sec. III C. In fact, $Z_a^{\mathbf{r}}$ should be a function of the observation time scale too, but we have neglected this dependence since the temperature variation of $Z_a^{\mathbf{r}}$ is of secondary importance here (see Sec. II B). The ansatz for $Z_a^{\mathbf{r}}$ adopted in Eq. (5) also subsumes the nonergodicity required to obtain a smoothly vanishing entropy in the $T=0$ limit from the continuous Gaussian distribution of minima.

The total number of minima in the crystalline and noncrystalline regions can vary independently via the parameters σ_x, $\sigma_{\rm shift}$, and σ_{nx}, and a Gaussian dependence is assumed for the number of minima as a function of the energy. The latter form is suggested by the central limit theorem and supported by previous results for a number of different model systems.[26,27,52,89–91] The variation of σ_a in Eq. (5) is therefore designed to sample a Gaussian distribution of minima at evenly spaced, nonextensive energy intervals. We ignore the permutation-inversion factor of $2N!$ in the partition function since it cancels out of the final expressions.

The value of $T_{3/4}$ determines how quickly $Z_a^{\mathbf{r}}$ reaches its high-temperature limiting value, and must be positive to prevent $Z_a^{\mathbf{r}}$ from diverging; the closer $T_{3/4}$ is to zero the more rapidly $Z_a^{\mathbf{r}}$ increases with T. When $T=T_{3/4}$ the regional configurational entropy achieves $\frac{3}{4}$ of its limiting value. The average potential energy of region $\underline{a}$ relative to the bottom of the region U_a^r is

$$U_a^r(T) = kT^2\frac{\partial \ln Z_a^{\mathbf{r}}}{\partial T} = \sigma_a NkT_{3/4}\left(\frac{T}{T+T_{3/4}}\right)^2. \quad (8)$$

The maximum value of U_a^r is $\sigma_a NkT_{3/4}$ and this must always be less than or equal to 2δ, the energy of the highest-lying minima in the region relative to the lowest, so $T_{3/4} \leqslant 2\delta/Nk\sigma_a$. The largest possible value of σ_a is $\sigma_{\max}=\sigma_x+\sigma_{\rm shift}+\sigma_{nx}$, and so we take $T_{3/4}\leqslant T_{3/4}^{\max}$, where $T_{3/4}^{\max}=2\delta/Nk\sigma_{\max}$. At $T=T_{3/4}$ we find $U_a^r(T_{3/4})=U_a^r(\infty)/4$.

In the present work we have taken the vibrational partition functions to be

$$Z_a^{\rm vib}(T) = (z_a^{\rm vib})^{3N-3} = \left[\frac{e^{-h\nu_a/2kT}}{1-e^{-h\nu_a/kT}}\right]^{3N-3},$$

$$Z_x^{\rm vib}(T) = (z_x^{\rm vib})^{3N-3} = \left[\frac{e^{-h\nu_x/2kT}}{1-e^{-h\nu_x/kT}}\right]^{3N-3}, \quad (9)$$

with

$$\nu_a = \nu_0 + \frac{\gamma(E_a/N+\delta)}{2\delta}. \quad (10)$$

Hence we have used $3N-6$ independent quantum-harmonic oscillators in an Einstein-type approximation where all the vibrational modes have the same frequency. For the crystal this frequency is ν_x, while for the noncrystalline regions the frequency varies from ν_0, for region one with $E_1=-N\delta$, to $\nu_0+\gamma$ for region $N+1$ with $E_{N+1}=N\delta$. ν_0, ν_x, and γ are further parameters of the model. Choosing $\gamma<0$ means that the higher energy non-crystalline minima exhibit lower frequencies, which is the behavior that we have found for finite clusters bound by a wide variety of different empirical potentials. However, bulk systems may be different: Sastry[52] has reported results for a binary Lennard-Jones system at constant volume that correspond to $\gamma>0$ behavior. The databases that we have generated for several bulk model atomic glass formers agree with Sastry's results and further indicate that $\gamma<0$ for Stillinger-Weber silicon,[92] while $\gamma\sim 0$ for two one-component Lennard-Jones systems,[32] again at constant volume. For $\gamma\neq 0$ the total partition function cannot be factorized into configurational and vibrational parts.

All thermodynamic properties were calculated using analytical derivatives of the appropriate partition function,[71] namely, $Z_x(T)$ for the crystal and $\Sigma_{a\ \rm connected} Z_a(T)$ for the liquid or glass. All the derivatives were checked numerically.

Variation of harmonic frequencies with the energy of the minimum is admitted via the parameter γ. Following the approach of Haarhoff[93] an anharmonic vibrational partition function can be written as[94]

$$Z_{\rm anharm}^{\rm vib}(i) = \left(\frac{kT(1+a_i kT)}{h\overline{\nu}}\right)^{3N-3}, \quad (11)$$

where E_i is the potential energy of minimum i, $\overline{\nu}$ is the geometric mean vibrational frequency and all the modes are assumed to have the same anharmonicity parameter a_i. The classical harmonic vibrational partition function is recovered if $a_i=0$. $Z_{\rm anharm}^{\rm vib}$ is incorrect in the low-temperature limit, because it is a classical expression. However, anharmonic effects are most likely to be important at high temperature, and the vibrational contribution to the entropy difference between the liquid and the crystal is then

$$\Delta S^{\rm vib} = k(3N-3)\ln\frac{\overline{\nu}_x(1+a_{nx}kT)}{\overline{\nu}_{nx}(1+a_x kT)} \to k(3N-3)\ln\frac{\overline{\nu}_x a_{nx}}{\overline{\nu}_{nx}a_x}, \quad (12)$$

where x and nx label the crystalline and noncrystalline parameters, respectively. Hence, in this high-temperature limit some allowance for anharmonicity can be made by changing the harmonic frequencies of the noncrystalline minima relative to ν_x. We will adopt this view rather than introduce any further parameters into the model. This approach does not mean that we believe anharmonicity is unimportant, but

rather that it can be incorporated in a first approximation by shifting the harmonic frequencies. In fact, the vibrational degrees of freedom play a key role in our interpretation of strong/fragile behavior, as for previous models.[52,95–98]

B. Dynamics

When combined with the thermodynamics of Sec. II A the model dynamics must satisfy the principle of detailed balance. Since we assume that rearrangements between regions are responsible for dynamical relaxation and transport properties we need only specify the transition rates $K_{a\leftarrow b}$ between them. This assumption is justified if there is a separation of time scales for transitions between regions compared to local equilibration. Because $T_{3/4}^{\max}$ is of order $1/N$, $Z_a^{\mathbf{r}} \approx \exp(N\sigma_a)$ above T_g. Hence the regional configurational partition functions are only weak functions of temperature above the glass transition, which is why we have neglected the dependence of $Z_a^{\mathbf{r}}$ upon the time scale. To simplify the analysis nonzero rates will only be admitted for regions that are ''adjacent'' in energy. We have checked that the inclusion of rearrangements between nonadjacent regions has little effect on the results. We therefore consider only

$$K_{1\leftarrow x},\ K_{x\leftarrow 1},\ K_{2\leftarrow 1},\ K_{1\leftarrow 2},\ldots,$$
$$K_{a-1\leftarrow a},\ K_{a+1\leftarrow a},\ldots,\ K_{N_r-1\leftarrow N_r}. \tag{13}$$

In the following derivation we continue to denote the regions as *a, b, c,* etc. and distinguish individual minima within a region by the subscripts *i, j,* etc. The rate of change of occupation probability for minimum *i* in region *a* is then

$$\frac{\partial P_i}{\partial t} = \sum_{j\neq i\in a} k_{i\leftarrow j}P_j - P_i \sum_{j\neq i\in a} k_{j\leftarrow i} + \sum_{j\notin a} k_{i\leftarrow j}P_j - P_i \sum_{j\notin a} k_{j\leftarrow i}, \tag{14}$$

and the rate of change of probability of occupation for region *a* is

$$\begin{aligned}\frac{\partial P_a}{\partial t} &= \sum_{i\in a}\frac{\partial P_i}{\partial t},\\ &= \sum_{i\in a}\sum_{j\neq i\in a} k_{i\leftarrow j}P_j - \sum_{i\in a} P_i \sum_{j\neq\in a} k_{j\leftarrow i} + \sum_{i\in a}\sum_{j\notin a} k_{i\leftarrow j}P_j - \sum_{i\in a} P_i \sum_{j\notin a} k_{j\leftarrow i},\\ &= \sum_{i\in a}\sum_{j\notin a} k_{i\leftarrow j}P_j - \sum_{i\in a} P_i \sum_{j\notin a} k_{j\leftarrow i},\\ &\equiv \sum_{b\neq a} K_{a\leftarrow b}P_b - P_a\sum_{b\neq a} K_{b\leftarrow a},\end{aligned} \tag{15}$$

where the last line defines $K_{a\leftarrow b}$:

$$K_{a\leftarrow b} = \frac{\sum_{i\in a}\sum_{j\in b} k_{i\leftarrow j}P_j}{\sum_{j\in b} P_j} = \frac{\sum_{i\in a}\sum_{j\in b} k_{i\leftarrow j}P_j}{P_b}. \tag{16}$$

$K_{a\leftarrow b}$ therefore depends explicitly upon the connectivity of the PES. We now factor $K_{a\leftarrow b}$ into an average vibrational contribution for transitions between individual connected minima in regions *a* and *b*, $k_{a\leftarrow b}$, and an exponential term containing the mean effective-free-energy barrier, ΔA (Fig. 1). For $k_{a\leftarrow b}$ we adopt a simple transition state theory form:

$$k_{a\leftarrow b} = \frac{kT}{h}\frac{Z_{ab}^{\mathrm{vib}\ddagger}}{Z_b^{\mathrm{vib}}},$$

with

$$Z_{ab}^{\mathrm{vib}\ddagger} = \begin{cases}(z_a^{\mathrm{vib}})^{3N-4}, & E_a > E_b,\\ (z_b^{\mathrm{vib}})^{3N-4}, & E_b > E_a.\end{cases} \tag{17}$$

The transition state is therefore assumed to have the same vibrational parameters as the minima in the higher energy region. Finally,

$$K_{a\leftarrow b} = \begin{cases}\dfrac{kT}{h}\dfrac{(z_a^{\mathrm{vib}})^{3N-4}}{Z_b^{\mathrm{vib}}}\exp\left[\dfrac{NT}{2}\left(\dfrac{\sigma_a-\sigma_b}{T+T_{3/4}}\right) - \dfrac{(\Delta A + E_a - E_b)}{kT}\right], & E_a > E_b\\ \dfrac{kT}{h}\dfrac{1}{z_b^{\mathrm{vib}}}\exp\left[\dfrac{NT}{2}\left(\dfrac{\sigma_a-\sigma_b}{T+T_{3/4}}\right) - \dfrac{\Delta A}{kT}\right], & E_b > E_a.\end{cases} \tag{18}$$

The first term in the exponential is included to ensure that the detailed balance condition $K_{a\leftarrow b}P_b = K_{b\leftarrow a}P_a$ is satisfied. In the limit of large N, $\sigma_b - \sigma_a$ is of order $1/N$, and so the argument of the exponential is intensive, not extensive, as it should be. After the self-consistent calculation of $Z(T,\tau)$ we obtain the thermodynamic properties by applying the usual relations of equilibrium thermodynamics. The probability flux out of region *a* is

$$\begin{aligned}f_a(T) &= P_a(T)\sum_{b\neq a} K_{b\leftarrow a}\Theta[f_b(T) - 1/\tau]\\ &= \sum_{b\neq a} K_{a\sigma b}P_b(T)\Theta[f_b(T) - 1/\tau],\end{aligned} \tag{19}$$

where the fluxes and probabilities are also implicit functions of the observation time scale, τ. In all the above derivations analogous expressions apply to the crystalline region with the appropriate parameters.

For the free-energy barrier between regions a and $a-1$ we take

$$\Delta A_a = \Delta A_{\max} - (\Delta A_{\max} - \Delta A_{\min}) \left(\frac{2a}{N} \right)^{\alpha}, \qquad (20)$$

For $\alpha > 0$ the free-energy barrier therefore increases as a decreases, and varies between $\Delta A_{\max}$ as $a \to 1$ at low temperature to $\Delta A_{\min}$ as $a \to N/2$ at high temperature. We neglect any explicit dependence of ΔA upon temperature for simplicity. ΔA subsumes the connectivity of the PES, allowing for larger potential or entropic barriers in lower-energy regions. Such a structure results when the PES is organized into multiple ''funnels,'' by which we mean sets of kinetically convergent pathways[36] terminating at different minima. Funnels that are deep in terms of potential energy will produce increasing effective activation barriers as the temperature falls, because the occupation probability shifts to lower-lying minima. Such topology probably also carries with it increasing entropic activation barriers, although entropic barriers could arise without large potential barriers. We have previously illustrated potential energy landscapes for a number of finite systems,[4,99] and future refinements of the present model will require further guidance from such calculations.

III. PROPERTIES OF THE MODEL

Nonexponential relaxation, a commonly observed property of glasses, is the expected behavior of a complex PES, because the analytical master equation solution of the dynamics is a sum of exponentials.[100,101] Nonexponential relaxation has already been demonstrated for at least two sorts of hierarchical model,[102,103] and observed in finite systems.[24] We will therefore concentrate on the temperature dependence of relaxation in the present work, along with the thermodynamic properties of our model. Even in other fields, where nonexponential relaxation is considered ''strange,'' new experiments that probe shorter time scales have revealed such properties.[104] Exponential relaxation is recovered in the master equation solution if all the exponents save one have decayed on the time scale in question.

A. Thermodynamics

Angell's classification of glass formers from ''strong'' to ''fragile'' [95,105,106] has now become standard notation. Dynamically, fragility is manifested by departure from Arrhenius kinetics in relaxation times, diffusion constants or viscosities and is fitted with the empirical Vogel-Tammann-Fulcher (VTF) equation[107–109] or other forms.[110] Thermodynamically, fragility is signalled by a large heat capacity difference between liquid and glass that leads to the Kauzmann ''paradox,'' where the extrapolated entropy of the supercooled liquid becomes equal to that of the crystal at the Kauzmann temperature $T_K > 0$.[111] The kinetic glass transition prevents this violation of the third law of thermodynamics, of course. In his influential paper, Kauzmann plots

$$[S_{\rm liquid}(T) - S_{\rm crystal}(T)]/[S_{\rm liquid}(T_m) - S_{\rm crystal}(T_m)] \equiv \Delta S(T)/\Delta S(T_m)$$

against T/T_m, and this is the form we will refer to as a ''K_m plot.'' Fragile and strong systems exhibit slopes greater or less than one in this plot, respectively, and a quantitative measure may be obtained from the initial slope at T_m:

$$\left(\frac{\partial \Delta S(T)/\Delta S(T_m)}{\partial T/T_m} \right)_{T=T_m} = \frac{T_m}{\Delta S(T_m)} \left(\frac{\partial \Delta S(T)}{\partial T} \right)_{T=T_m} = \frac{T_m}{\Delta S(T_m)} \frac{\Delta C(T_m)}{T_m} = \frac{\Delta C(T_m)}{\Delta S(T_m)} \equiv \frac{\Delta C(T_m) T_m}{\Delta U(T_m)}, \qquad (21)$$

where U is the internal energy and C the heat capacity. [For a system at constant pressure the enthalpy H rather the internal energy U appears in Eq. (21).] We immediately conclude that, by this definition, thermodynamically fragile systems have some combination of a larger heat capacity or smaller internal energy difference between liquid and crystal or a higher melting point. Within the present model, parameter changes that affect $\Delta C(T_m)$ or $\Delta U(T_m)$ can be more than compensated for by a change in T_m. Hence some caution is needed in making predictions from Eq. (21). An alternative definition of thermodynamic fragility, which uses T_g rather than T_m as a reference point,[112] will be discussed below.

To explain the relations between thermodynamic properties and changes in parameter values it is helpful to consider the behavior of $\Delta S^{\rm eq}(T)$, the entropy difference between the hypothetical ergodic noncrystalline phase space and that of the crystal. $S^{\rm eq}_{nx}$ is calculated from $Z^{\rm eq}_{nx}(T) = \lim_{\tau \to \infty} Z_{nx}(T, \tau)$:

$$Z^{\rm eq}_{nx} = \sum_{a=1}^{N_r} Z_a(T). \qquad (22)$$

For the present model the general appearance of $\Delta S^{\rm eq}(T)$, neglecting vibration, is shown in Fig. 2. $\Delta S^{\rm eq}/Nk$ decreases from its high-temperature limit of $\sigma_{\rm shift} + \sigma_{nx}$ and starts to fall rapidly around T_{fs}, because the regions where the energy density of minima (and σ_a) is largest have decreasing occupation probabilities. When only the lowest-energy region has a significant occupation probability, $\Delta S^{\rm eq}(T)/Nk$ decreases slowly from a plateau value of $\sigma_{\rm shift}$ until T approaches absolute zero, where $Z^{\mathbf{r}}_a(T)$ finally tends to unity. It is only in this limit, where T approaches $T_{3/4}$, that the temperature dependence of $Z^{\mathbf{r}}_a(T)$ is significant. Hence, the Kauzmann paradox is naturally avoided even without ergodicity breaking in the noncrystalline phase space.

If $h\nu_0$ and $h\nu_x$ are large compared to kT_m then the vibrational contribution to $\Delta S^{\rm eq}(T)$ decays to zero above T_m and has little effect. On the other hand, in the low-frequency limit the plateau value of $\Delta S^{\rm eq}(T)/Nk$ is shifted to

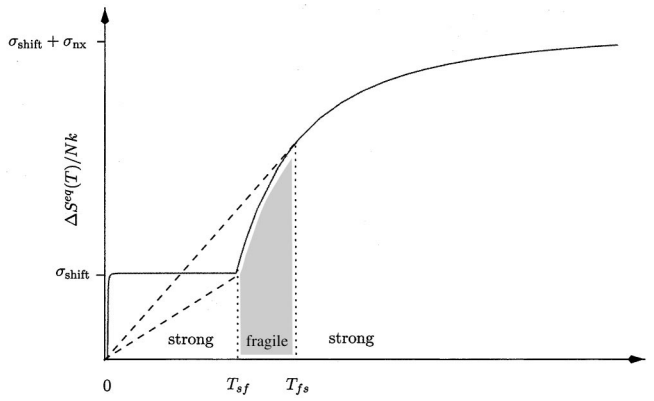

FIG. 2. Generic form for $\Delta S^{\text{eq}}(T)$ excluding vibration (solid line) to illustrate how the thermodynamic strength or fragility defined by the K_m-plot (K_g-plot) slope depends on the position of T_m (T_g) with respect to T_{sf} and T_{fs}. The dashed lines touch the ΔS^{eq} curve at the points where $\partial\Delta S^{\text{eq}}/\partial\Delta T=\Delta S^{\text{eq}}/T$. If T_m (T_g) lies within the shaded region the system is thermodynamically fragile, by the K_m-plot (K_g-plot) definition, because the slope is greater than unity.

$3\ln\nu_x/\nu_0+\sigma_{\text{shift}}$. In fact, vibrational properties are not expected to vary strongly between crystalline and noncrystalline minima,[84] although we will argue below that they should be correlated with the number of minima, and play an important role in determining the kinetic fragility.

The results in Sec. IV show that the main effect of including kinetic disconnection of regions is to shift the plateau in Fig. 2 above the limit of σ_{shift} for the ''equilibrium'' glass as the observation time scale decreases. The shift simply results from freezing into a higher-energy region with $0<\sigma_a-\sigma_x-\sigma_{\text{shift}}<\sigma_{nx}$ and lower vibrational frequencies (for $\gamma<0$).

The key temperatures in Fig. 2 are T_{sf} and T_{fs}, where ΔS^{eq} satisfies

$$\partial\Delta S^{\text{eq}}/\partial T=\Delta S^{\text{eq}}/T. \tag{23}$$

If $T_{sf}<T_m<T_{fs}$ the system is thermodynamically fragile, whereas if $T_m<T_{sf}$ or $T_m>T_{fs}$ then the system is thermodynamically strong, according to the K_m-plot definition. We expect real strong liquids to correspond to the category $T_m>T_{fs}$ because $T_m<T_{sf}$ corresponds to a situation where the system has reached the bottom of the noncrystalline configuration space at T_m. Therefore, T_m/T_{fs} is a key quantity in determining the position of the system with respect to the physically realistic zone of thermodynamically strong behavior, and, if we ignore the parameter space with $T_m<T_{sf}$, we can say that the thermodynamic strength of the liquid increases as T_m/T_{fs} increases, by the K_m-slope definition.

For larger $T_{3/4}$ the final steep decay of ΔS^{eq} to zero in Fig. 2 occurs at higher temperature, but the upper bound to $T_{3/4}$ imposed by internal consistency of the model prevents values of $T_{3/4}$ that would give qualitatively different behavior. σ_x and E_x do not affect the plot at all. In contrast, T_{sf} and T_{fs} scale roughly as δ/σ_{nx}, with $kT_{sf}\sim\delta/2\sigma_{nx}$ and $kT_{fs}\sim\delta/\sigma_{nx}$. The effect of the vibrational entropy is discussed in Sec. IV for parameters appropriate to two different systems.

The above analysis enables us to predict how the form of a K_m plot, where the horizontal axis is T/T_m rather than T, will change with the model parameters. Neglecting vibration, and using the maximum term approximation described in the Appendix,

$$kT_m=\frac{-E_x+\sqrt{E_x^2-\delta^2}}{2\sigma_{nx}}, \tag{24}$$

if $\sigma_{\text{shift}}=0$, so moving E_x to lower energy increases T_m almost linearly. Hence decreasing E_x can shift T_m above T_{fs} and change fragile thermodynamics to strong. In the same approximation the equilibrium glass temperature T_g^{eq} can be estimated from the condition $P_1(T_g^{\text{eq}})=P_2(T_g^{\text{eq}})$, giving $kT_g^{\text{eq}}=\delta/2\sigma_{nx}\approx kT_{sf}$.

In Sec. IV we will illustrate how the K_m slope of one parameter set can be changed from fragile to strong simply by decreasing E_x. Ito, Moynihan, and Angell[112] have suggested that a more useful indication of thermodynamic fragility might be obtained from plotting $\Delta S(T_g)/\Delta S(T)$ against T_g/T, and we will refer to this representation as a K_g plot. The slope of this plot at T_g is $\Delta C(T_g)/\Delta S(T_g)$, and the strong/fragile character is now determined by comparing T_g with the solutions of Eq. (23), instead of T_m. The correlation between dynamics and thermodynamics is preserved when the K_g-plot definition is used for the parameter sets that we have considered with $\gamma<0$ (Sec. IV). Another possibility would be to use the crossover temperature from Arrhenius to super-Arrhenius behavior, as discussed by Tarjus, Kivelson, and Viot.[113] This crossover temperature might be less ambiguous than the kinetically defined T_g, but we have not considered it here.

Accurate analytical expressions for thermodynamic functions corresponding to the hypothetical equilibrium noncrystalline phase space are presented in the Appendix. These results help to explain how the thermodynamics of the model vary with the parameters. For example, we find that the jump in the heat capacity at T_g is proportional to the number of noncrystalline minima.

B. Dynamics

In addition to the K plots defined above we will also present plots of the liquid/glass entropy and heat capacity per atom against T/T_m (''S plot'' and ''C plot,'' respectively), along with a plot of $\log_{10}$ (relaxation time) against T_g/T (''t plot''). A proper calculation of a relaxation time or diffusion constant would require detailed assumptions about the possible rearrangements that the system can undergo. Instead we proceed on the basis that intra-region dynamics do not contribute to the relaxation times in question, or to diffusion, and use

$$t\sim 1\Big/\sum_a f_a. \tag{25}$$

We therefore take the relaxation time to be inversely proportional to the sum of probability fluxes out of (or into) each region.

In previous work we have investigated relaxation (of the total energy) in a number of atomic and molecular clusters using a master equation approach[100,101] following Kunz and co-workers.[9–12] Non-Arrhenius relaxation of the total potential energy has been observed for systems with multifunnel energy landscapes.[4,24,25] We have suggested that the apparent increasing activation energy with decreasing temperature is due to the system occupying lower-energy states within different funnels that can only transfer probability via their higher energy members. In other words, the transition states in question do not change, but the occupation probability shifts to lower potential energy within each funnel. This situation is subsumed here in the general form adopted for the effective free-energy barrier in Eq. (20). The shift of population density to the bottom of deep kinetic traps would probably entail both larger potential and entropic barriers. Equation (20) can also model the situation where the barriers are principally entropic, and caused by a scarcity of relaxation pathways as the energy density of minima decreases. The details of the relaxation mechanisms, such as the degree of cooperativity, need not be known in the present analysis.

A simple analytical expression for the relaxation time t can again be obtained, as described in the Appendix. We find that the t-plots should have intercept $-\log_{10}\nu_0$ and initial slope $(\Delta A_{\min}+\delta)T_g \log_{10} e/k$.

C. Residual entropy

By construction, the entropy of the present model always tends to zero as $T\rightarrow 0$, whether the system freezes to a crystalline or a noncrystalline region. The number of connected regions decreases with temperature, and then, after freezing to one region, the system settles into a single local minimum as the temperature is further reduced. The internal energy tends to $E_a-\delta$ as $T\rightarrow 0$, and so the system always relaxes to the bottom of a region in this model, which we have assumed to consist of a single minimum (aside from trivial permutational isomerism). There is no residual entropy because in these calculations we can track the relaxation of the system down to its final resting place and calculate the thermodynamic properties directly from the partition function.

Residual entropy must be included for equilibria where one phase is dynamically interconverted into any one of a number of different possible glasses. Bowles and Speedy have analyzed this situation in detail for the vapor pressure of a glassy crystal composed of rigid dimers.[114] The entropy corresponding to the number of different glasses in equilibrium with the vapor must be included to produce the correct vapor pressure.[115,116] In the classic experiment of Eastman and Milner[117] the thermodynamic properties of substitutionally disordered AgCl/AgBr crystal ''solutions'' were compared using electrochemical and heat capacity measurements. The results are only consistent if the permutational near degeneracy of the different crystals is added to the entropy obtained from calorimetry. The difference arises because the electrochemical measurements involve a dynamical equilibrium in which the effects of ergodicity breaking are undone, whereas the heat capacity measurements are for a particular realization of the mixed crystal.

Standard thermodynamics can be applied to calculate the change in entropy of a glass with temperature so long as ergodicity is not restored.[117–119] Choosing the reference state at $T=0$ with zero entropy is consistent with the statistical entropy of the accessible phase space corresponding to a single local minimum.[114] The third law may then be expressed as ''the entropy of any body tends to zero at the absolute zero of temperature.'' [114] This is the view that we have adopted in the present work. The alternative ''thermodynamic'' approach is to define the entropy experimentally from an ideal gas reference state, but then the entropy of the glass is finite at $T=0$.

IV. RESULTS

Our initial choice of parameter values was guided by results for supercell calculations on a system containing 216 silicon atoms modeled by the Stillinger-Weber potential.[92] The calculations employed reduced units with $h=k=1$ and energies in ϵ, where ϵ corresponds to the pair well depth. Frequency parameters are therefore in units of ϵ/h and energy parameters are in ϵ. To convert from reduced units we have taken $\epsilon=3.473\,92\times10^{-19}$ J, the value for Stillinger-Weber silicon.[92] For the latter system $h\nu/\epsilon\approx 0.019$ for the geometric mean normal mode frequency of minima with crystalline character, while the variation of $\overline{\nu}$, the geometric mean frequency, for the noncrystalline minima can be represented by $\nu_0=0.017$ and $\gamma=-0.0011$ to a first approximation. The crystal has $E_x/\epsilon=-2$ while the noncrystalline minima have energies per atom in the range -1.83 to -1.89ϵ. With an energy origin in the middle of the noncrystalline minima, these results correspond to $\delta=0.03$ and $E_x=-0.08$. We have also considered parameters deduced from a sample of stationary points obtained for a binary Lennard-Jones system,[32] and we will comment on the results below. Empirically, the binding energy lost on melting in a wide range of materials varies from around 4–10%,[120] suggesting bounds for physically reasonable values of E_x. Alternatively, Stillinger has noted that the change in potential energy on melting accounts for around 80% of the latent heat in

TABLE I. Variable parameters for the results discussed in Sec. IV.

Sample	Fig.	σ_{nx}	δ	$\nu_{\max}$	ν_x	E_x	$\Delta A_{\max}$	$\Delta A_{\min}$
F	3	2.00	0.0375	0.017	0.020	−0.05	0.5	0.0
S	4	0.15	0.0100	0.010	0.011	−0.03	1.5	1.0
FS	5	2.00	0.0375	0.017	0.020	−0.08	0.5	0.0
SF	6	0.15	0.0100	0.010	0.011	−0.03	2.0	0.1

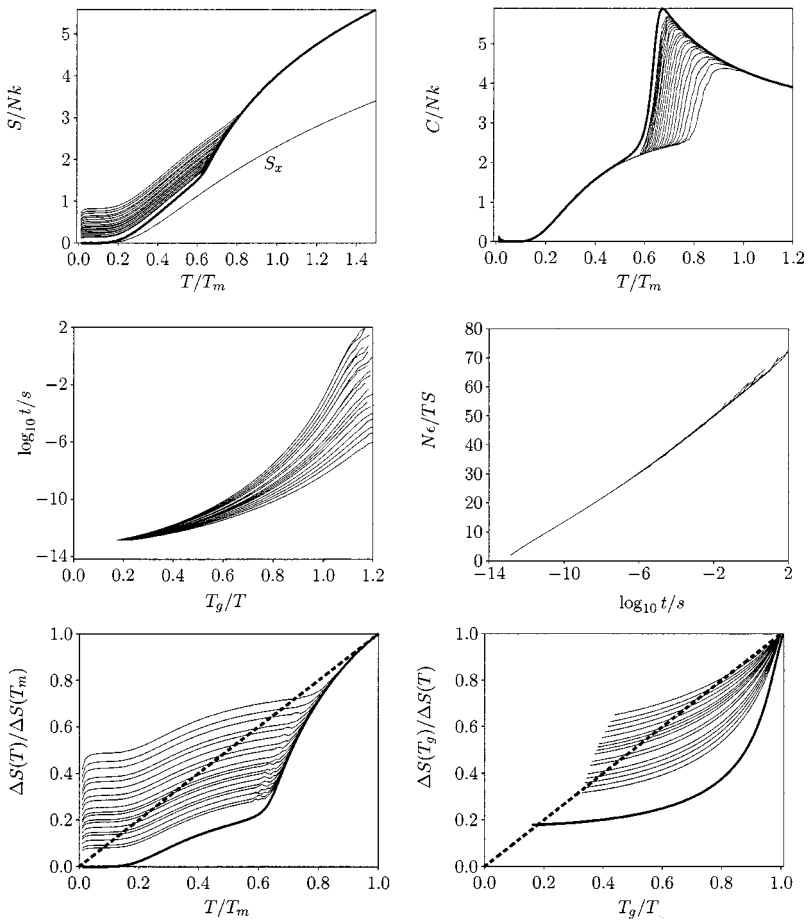

FIG. 3. Results for parameter set *F* (see Table I).

models of bulk Lennard-Jonesium and water.[6,84,121]

Although the number of minima is not an experimental observable we can deduce sensible values for the σ parameters from heat capacity data. Despite the fact that vibrational and configurational contributions are not strictly separable, the magnitude of the heat capacity peak at T_g implies that σ_{nx} is of order unity. We held the following parameters fixed for all runs: $N=400$, $\alpha=0.25$, $\sigma_{\rm shift}=0$, $\sigma_x=0$, and $T_{3/4}=T_{3/4}^{\rm max}$. The results do not change significantly if $T_{3/4}=0$ is used instead of $T_{3/4}^{\rm max}$.

The effect on the dynamics of systematically varying a single parameter while keeping the others fixed was first investigated. A necessary condition for non-Arrhenius dynamics in the present model is that ΔA increases with decreasing potential energy. We were not able to obtain significant non-Arrhenius character without this condition, as discussed below. For non-Arrhenius dynamics to be observed on a given time scale it is also necessary for the system to reach the regions where the barriers increase significantly, before kinetic arrest occurs. Large σ_{nx} and small δ produce a lower $T_g^{\rm eq}$, and from Eq. (A2) we see that this effect is coupled to a slower decrease in a^* as the temperature falls, where a^* is the most probable region (see the Appendix). However, Eqs. (A4) and (A5) for the relaxation time also contain the ratio δ/σ_{nx}. The effect of varying σ_{nx} on its own is unambiguous. The system freezes into a higher-potential-energy region for larger σ_{nx} because only the smaller non-Arrhenius terms in the flux are affected [equation (A5)], while a^* varies more slowly with T [Eq. (A2)]. The effect of varying δ can depend upon the fixed values of the other parameters. Decreasing δ decreases the relaxation time [Eq. (A5)], and so T_g decreases. However, decreasing δ also means that a^* varies more slowly with temperature. Usually we find that decreasing δ produces stronger dynamics since the latter effect dominates.

Increasing ν_0 can change strong dynamics to fragile by decreasing the relaxation time [Eqs. (A4) and (A5)], enabling the system to relax further down the PES before freezing. Increasing $\Delta A_{\rm min}$ has the opposite effect, since the relaxation time increases. The dynamics are less sensitive to the value of $\Delta A_{\rm max}$, and increasing $\Delta A_{\rm max}$ for fixed $\Delta A_{\rm min}$ can produce more fragile behavior because the difference $\Delta A_{\rm max}-\Delta A_{\rm min}$ appears in the leading non-Arrhenius term in Eq. (A5) and determines the variation in barrier height with a in Eq. (20).

TABLE II. Properties of the data sets in Table 1. The K_m and K_g slopes are the slopes of the K_m and K_g plots at $T=T_m$ and $T=T_g^{\rm eq}$, respectively, for the equilibrium liquid. $T_{3/4}^{\rm max}=T_g^{\rm eq}/100$ in each case.

Sample	T_m	$T_g^{\rm eq}$	K_m slope	K_g slope
F	0.0150	0.0094	1.02	3.62
S	0.0612	0.0333	0.23	0.36
FS	0.0296	0.0094	0.19	4.74
SF	0.0613	0.0333	0.23	0.36

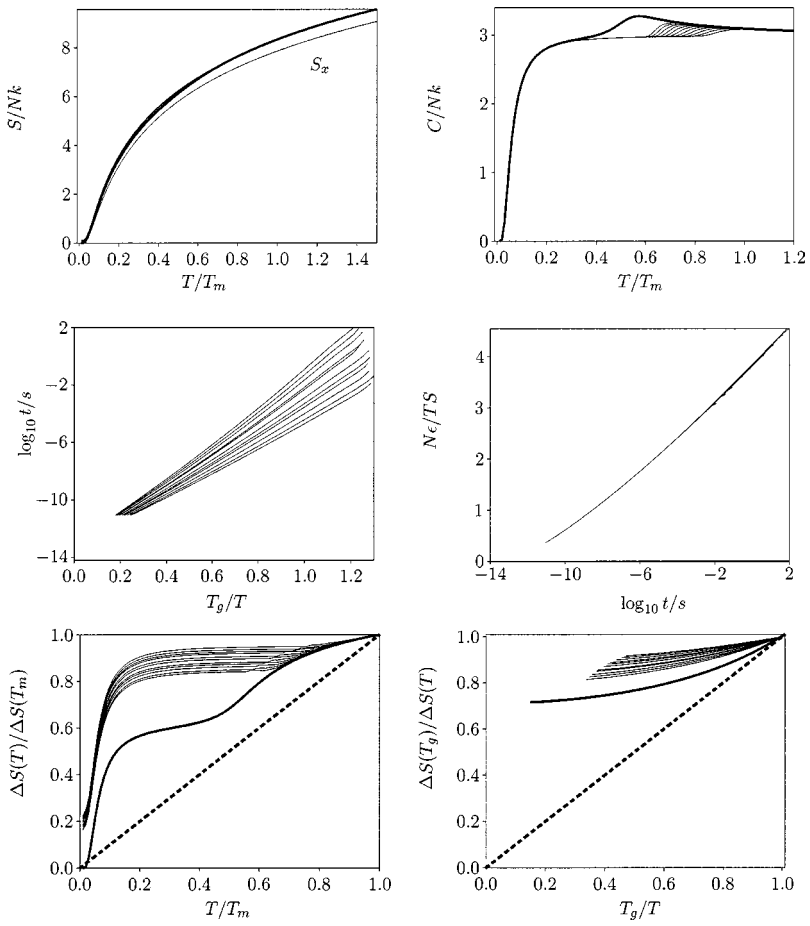

FIG. 4. Results for parameter set *S* (see Table I).

At first sight, the stronger dynamics observed for larger σ_{nx} seem to break the correlation between dynamics and thermodynamics, because increasing σ_{nx} should produce a larger heat capacity peak at T_g, making the system thermodynamically more fragile. In reality, variations of σ_{nx} should probably be strongly correlated with variations in ν_0. For example, in a series of 13-atom clusters bound by a variable-range potential the geometric mean frequency, averaged over minima, increases almost linearly with the number of minima.[22] The total entropy is therefore expected to *decrease* as the number of minima increases: the loss of accessible configuration space associated with a shorter range potential produces a larger number of *narrower* potential wells. When ν_0 is varied with σ_{nx} in this manner, fragile dynamics are found to be associated with larger σ_{nx}. Significant thermodynamic features in the heat capacity and entropy at T_g are then correlated with non-Arrhenius dynamics, but it is still possible to break this correlation, as discussed below.

The Adam-Gibbs result[47] that $\ln t$ should be inversely correlated with the product of temperature and configurational entropy, is only meaningful in the present model if $\gamma=0$, when the vibrational contribution can be factored out. Even in this case the relation does not hold very well, because the configurational entropy does not tend to zero at T_g, but instead we find a strong correlation between $\ln t$ and $1/TS$ for the total entropy. We therefore include such plots in the results discussed below. It is interesting to contrast this result with the scaling law connecting diffusion with entropy, which holds quite well for a variety of liquids above the melting point.[122] Several recent simulation studies suggest that the original Adam-Gibbs formulation deserves further consideration,[51–53] but we leave further analysis for future work.

The results for four specific parameter sets will now be discussed in more detail. The variable parameters are specified in Table I (see Figs. 3–6), and some of the thermodynamic properties are listed in Table II. We ran calculations for observation times corresponding to regular intervals on a $\log_{10}$ scale covering more than ten decades. The longest observation time was chosen to be 100 s for comparison with previous work.[106] For each choice of parameters the melting temperature T_m was first determined, and the calculations of thermodynamic properties and rates were then started from $T=3T_m$, decreasing T in steps of order $0.01T_m$. T_m was calculated by numerical solution of the condition for equal Helmholtz free energy:

$$Z_x(T)=\sum_{a=1}^{N+1} Z_a(T). \tag{26}$$

In fact, this scheme gives T_m for the hypothetical ergodic noncrystalline phase space. For consistency we should perhaps recompute T_m for each time scale considered using the nonergodic partition functions. This procedure would be more time consuming, since it would require a calculation of the fluxes for each increment in the continuous temperature

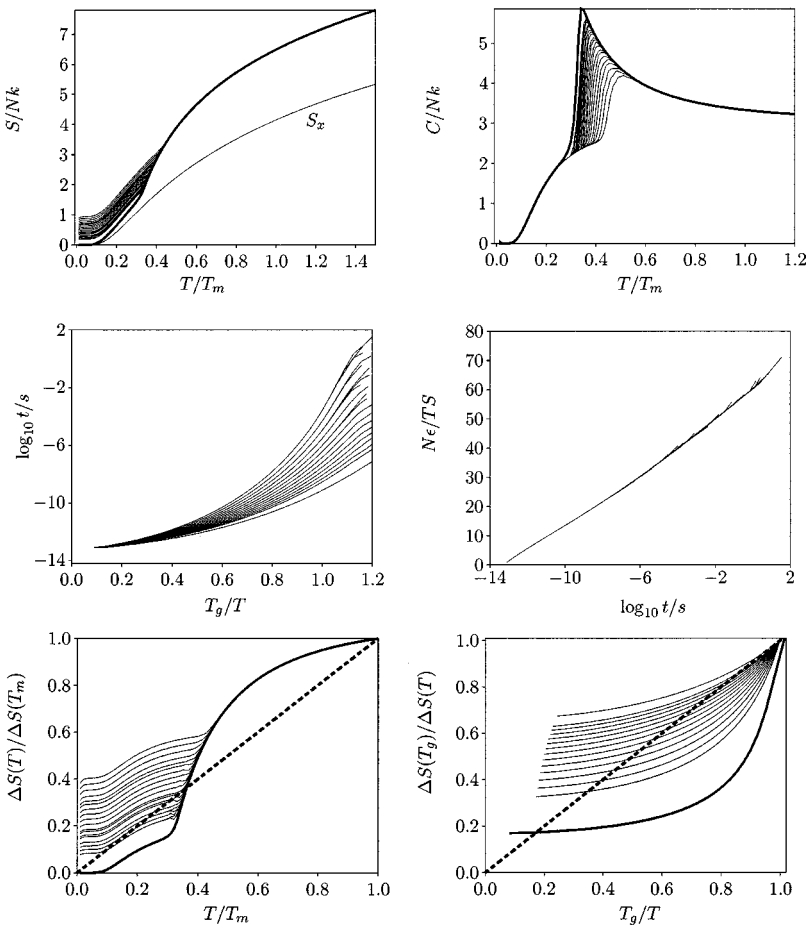

FIG. 5. Results for parameter set *FS* (see Table I).

variable. Fortunately, however, it is not necessary, because the ergodic and nonergodic values of the free energy are practically identical at T_m for the present model. The largest deviations occur for the shortest time scales, and amount to just 0.3% for the worst case. The dependence of T_m on the observation time scale is therefore negligible.

In each figure are superimposed the results for up to 20 observation time scales. In each case T_g, the entropy of the noncrystalline state, and the temperature of the heat-capacity peak increase smoothly, and the maximum relaxation time decreases smoothly, as the observation time scale decreases. In the K_m and K_g plots the curves shift smoothly up the vertical axis as the observation time increases, while the plots of $\log_{10} t$ against $1/TS$ are relatively insensitive to τ. If the T_g scaling of the horizontal axis is omitted in the *t*-plots then the curves for different observation time scales lie on top of one another. It is noteworthy that $\log_{10} t$ correlates quite well with $1/TS$, since this relation was not explicitly built into the model.

In the *S*-plots we include the entropy of the crystal S_x for reference. We also indicate the infinite time scale limit for the noncrystalline phase space by a bold line in the *S*, *C*, K_m, and K_g plots. A straight dashed line is drawn from the origin to the point (1, 1) in the *K* plots to divide strong and fragile behavior according to the K_m- or K_g-plot definition. For the *t* and K_g plots we assigned T_g as the temperature of the heat capacity maximum, which lies systematically above the temperature at which freezing to a single region occurs. Hence the T_g/T scale extends beyond unity in the *t*-plots.

In each K_m and K_g plot there is a gap between the bold curves corresponding to equilibrium within the noncrystalline phase space, and the longest time scale results. This is because, even on the longest observation time scale of 100 s, the system fails to reach the lowest-energy liquid region, but instead freezes into a higher-energy region [Fig. 7(b)]. For systems *F*, *S*, *FS*, and *SF* the lowest-energy regions frozen into are 7, 39, 10, and 38, respectively. The free energy, internal energy and entropy have almost their equilibrium values until T_g is reached. At this point the system freezes to one region, and changes to the partition function caused by shifts in the probability distribution between regions are lost.

Parameter set *F* produces fragile behavior, with a large peak in the heat capacity at T_g, an obvious change of slope in the entropy at T_g, K_m-plot and K_g-plot slopes greater than one, and non-Arrhenius variation of the estimated relaxation time (Fig. 3). In contrast, parameter set *S* produces strong behavior, with small features in the heat capacity and entropy at T_g, K_m-plot and K_g-plot slopes closer to zero, and an essentially Arrhenius relaxation time. As anticipated in Sec. III A, decreasing E_x from parameter set *F* can change the appearance of the K_m plot to strong (system *FS*, Fig. 5), but hardly changes the other plots. These results show that the K_m plot is probably not a useful diagnostic, and that the K_g plot suggested by Ito, Moynihan, and Angell[112] may be

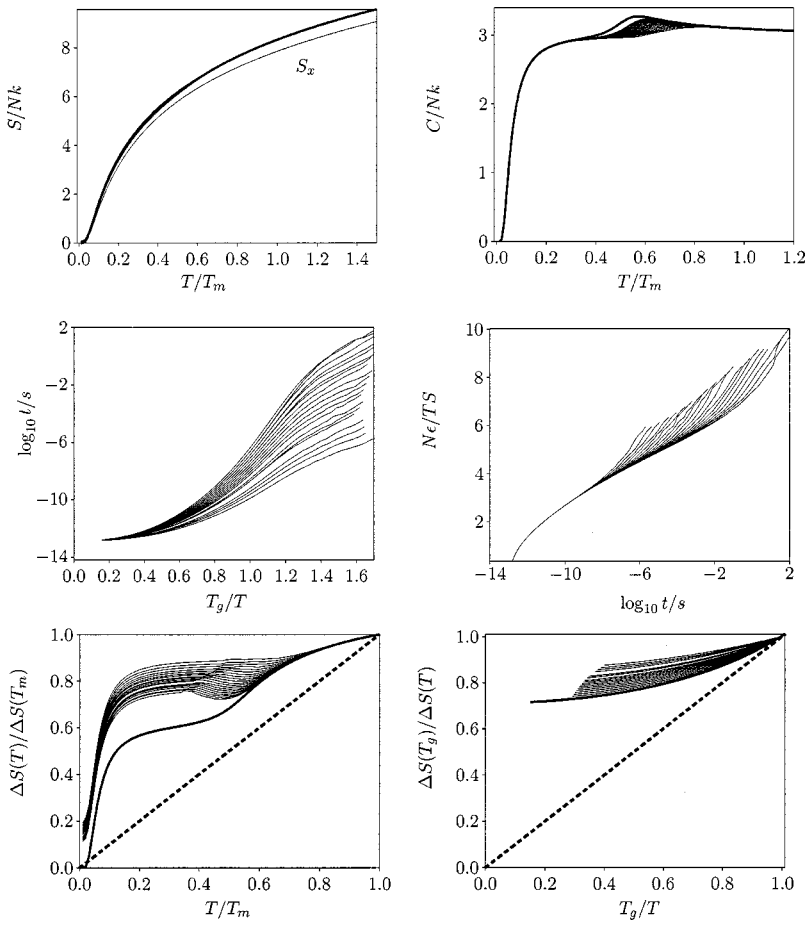

FIG. 6. Results for parameter set *SF* (see Table I).

better because it remains fragile for system FS. However, we note that the K_g-plot slope also depends upon the time scale of observation, τ, and decreases with decreasing τ.

Lowering the free energy barriers from parameter set *S* enables that system to access lower regions of the PES before kinetic arrest, and produces non-Arrhenius behavior in the *t* plot (system *SF*, Fig. 6). Hence, in the present model, strong behavior in the relaxation dynamics properties also requires either activation barriers that do not increase with decreasing potential energy, or sufficiently high barriers for the system not to access lower parts of the surface before freezing. It is possible that these properties may be linked with a smaller number of minima, but further exploration of bulk potential-energy surfaces is needed to analyze this effect.

Sastry, Debenedetti, and Stillinger studied the average energy of the occupied minima as a function of temperature and cooling rate[123] for a binary Lennard-Jones glass. The corresponding quantity as a function of observation time scale is easy to calculate in our model and is given by $E_{\min}(T,\tau)=\Sigma_a(E_a-\delta+U_a^r)P_a/N$, where the energy is per atom. Two such plots are given in Fig. 7.[123] As expected, we find that the lowest energy achieved increases as the observation time decreases. Similar results have also been found for another binary Lennard-Jones system[124] and for silica.[125] $E_{\min}^{\mathrm{eq}}$, the average minimum energy for the ergodic noncrystalline phase space, is plotted in Fig. 8 for each parameter set. For parameter set *F*, which is the only one to exhibit a fragile K_m plot, $E_{\min}^{\mathrm{eq}}/\delta$ is significantly lower at T_m than for the other examples. The extent to which $E_{\min}^{\mathrm{eq}}$ has relaxed at T_m correlates with the entropy difference $\Delta S(T_m)$ in Eq. (21), and with the K_m-plot slope, if $\Delta C(T_m)$ is constant. We also expect it to correlate with the degree of non-Arrhenius behavior, when increasing barriers are present.

Sastry, Debenedetti, and Stillinger inferred an increase in barrier height as the system relaxed to lower regions of the PES from their simulations.[123] The activation energy derived from the α-relaxation time for this system shows a corresponding increase.[123] It is likely that these barriers and activation energies correspond to the effective activation energies for transitions between regions, rather than barriers for transitions between individual minima. This interpretation is supported by detailed calculations of minima, true transition states, and rearrangement pathways for the same system,[32] and by recent simulations where the dynamics of transitions between minima are followed closely.[126]

In another contribution, Sastry has suggested an expression for fragility, which depends upon the number of local minima, their distribution, and the change in their vibrational properties as a function of energy.[52] In his model the free-energy barrier for diffusion is assumed to be inversely proportional to the configurational entropy, and therefore increases with decreasing temperature. Our results for a large database of minima corresponding to the same system suggest that $\nu_0=0.061$, $\gamma=0.0017$, $\delta=0.06$ are reasonable pa-

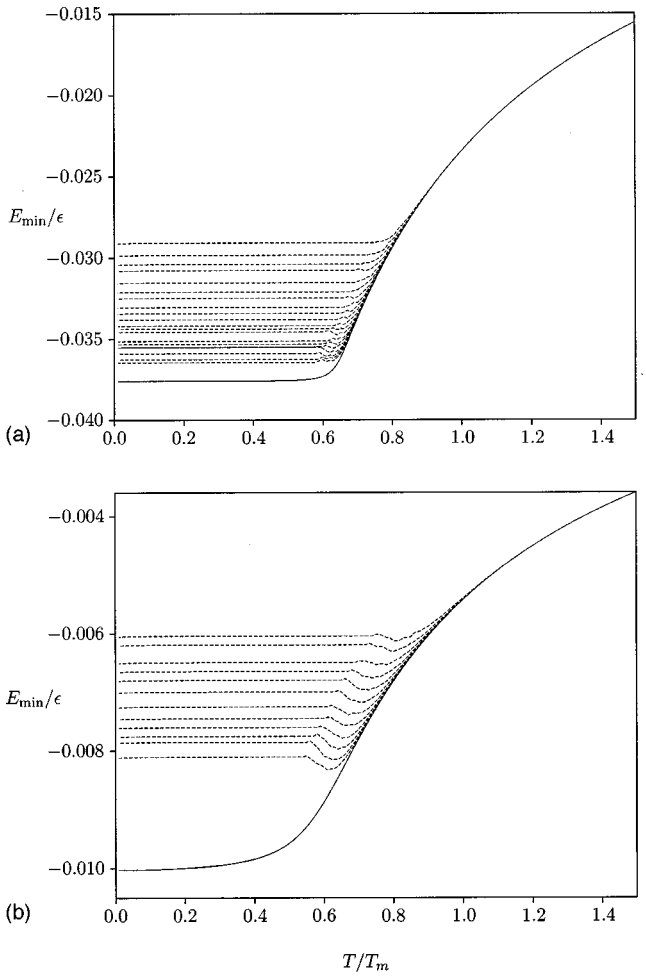

FIG. 7. $E_{\min}(T,\tau)$ for parameter sets (a) *F* and (b) *S* in Table I. The series of lines correspond to different values of τ, and the bold line is for the equilibrium liquid.

rameters in this case, if we use the same mass and ϵ as for Stillinger-Weber silicon. The frequencies are therefore significantly larger for the same binding energy ϵ and increase rather than decrease as the energy of the minima rises. The energy range spanned by the minima is also significantly larger, in terms of reduced units. When such parameters are used in the present model we first observed that the larger frequencies lead to relaxation to the bottom of the noncrystalline minima unless the observation time scale is lowered or the free energy barriers are increased. We set $\nu_x=\nu_0$ and adjusted E_x to obtain heat capacity maxima at about the same values of T/T_m as for the parameter sets *F*, *S*, *FS*, and *SF*. We found that the *S*, *C*, and *t* plots were largely unaffected, but that the K_m and K_g plots changed from strong to fragile in character for *S* and *SF*. The plots of $1/TS$ versus $\log_{10} t$ become less straight for the adjusted *F* and *FS*.

When $\gamma>0$ the vibrational entropy favors lower-lying minima, and so it is not surprising that the rate of entropy loss from the supercooled liquid is faster, and that the K_m, and K_g plots appear more fragile. For the adjusted parameter sets *S* and *SF* the fragile K_m and K_g plots become inconsistent with the appearance of the *S* and *C* plots, which remain strong in character due to the low energy density of minima.

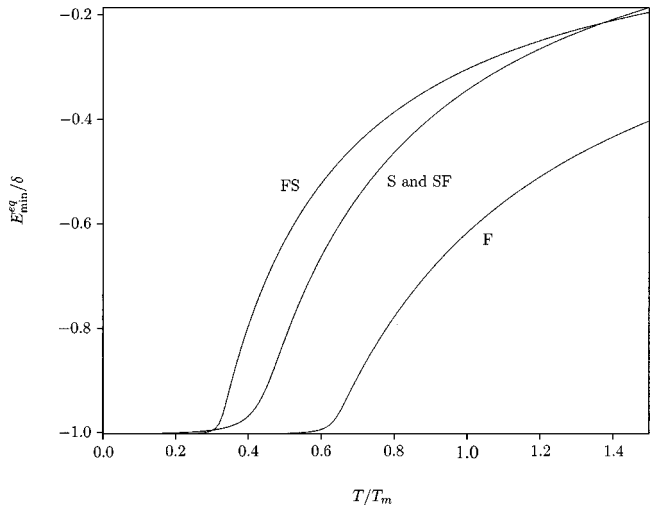

FIG. 8. $E^{\rm eq}_{\min}(T)/\delta$ for the four parameter sets listed in Table I, as labeled. $E^{\rm eq}_{\min}=-\delta(1+1/N)$ corresponds to the bottom of the liquid/glass configuration space.

We were unable to obtain non-Arrhenius behavior for the dynamics without allowing the free-energy barriers to increase with decreasing potential energy: the sign of γ does not play a crucial role in our model.

V. CONCLUSIONS

The dynamics and thermodynamics of a simple but nontrivial potential energy surface (PES) support a rich variety of behavior with a clear physical basis. Although the most recent definition of a fragility metric considers only data that are readily obtained by simple differential thermal analysis,[106] and the classification of some commonly used systems may still be controversial,[113] there are still associated expectations of the thermodynamics corresponding to strong and fragile dynamics. The present results suggest that fragility is associated with a larger number of local minima, lower effective potential energy barriers, and higher vibrational frequencies, in good agreement with Angell's previous interpretation.[95]

A necessary condition for non-Arrhenius dynamics is that the free-energy barrier to relaxation increases as the potential energy decreases, which is the expected behavior for a multifunnel potential energy surface that becomes increasingly underconnected at low energy.[4] However, for non-Arrhenius dynamics to be observed it is also necessary for the system to sample regions with increasing barriers on the given observation time scale. Lower free-energy barriers and higher frequencies can therefore lead to more fragile dynamics simply because the system relaxes to deeper regions of the PES on a given time scale. Increasing the energy density of minima alone produces more fragile thermodynamics but stronger, more Arrhenius, dynamics. However, systems with more minima are expected to have higher vibrational frequencies, and this effect can make the dynamics more fragile by increasing transition rates and lowering the relaxation time.

Increasing pressure (or density) is expected to reduce the number of local minima,[127,128] and should also increase vibrational frequencies. The present model therefore predicts

that higher pressure or density will lead to more fragile dynamics, since the system can then access lower-energy regions of the PES associated with deeper kinetic traps. This prediction is in agreement with experimental data for silica[95] and simulation results for the binary Lennard-Jones system.[52] However, the model also suggests that the magnitude of the heat capacity peak associated with the glass transition should decrease.

The alternative calibration of thermodynamic properties using T_g, suggested by Ito, Moynihan, and Angell,[112] correlates better with dynamical properties than the usual scaling based on T_m. However, it is still possible to obtain systems with strong thermodynamic characteristics but fragile dynamics if the free-energy barriers are small enough for the system to access low-lying regions of the potential-energy surface. Future surveys of potential energy surfaces will help to guide further development of the model, and may also help to distinguish between different theories.[63,64,129–131]

ACKNOWLEDGMENTS

We gratefully acknowledge helpful discussions with Professor A. Angell and Professor M. Dzugutov. J.P.K.D. is grateful to Emmanuel College, Cambridge for financial support.

APPENDIX: ANALYTICAL RESULTS FOR THERMODYNAMIC AND DYNAMIC PROPERTIES OF THE MODEL

Accurate analytical expressions can be derived for the hypothetical equilibrium noncrystalline phase space simply by replacing all the sums over regions with the term corresponding to region a^*, which is defined as the maximum term in the partition function sum. This maximum term approximation is appropriate in the limit of large N, where the product of the Boltzmann factor and the number of minima is sharply peaked. For $\gamma=0$, where the vibrational and configurational contributions are separable:

$$\frac{A^{\mathrm{eq}}_{nx}}{N}=\frac{3h\nu_0}{2}+3kT\ln\left(1-\frac{1}{\xi}\right)\times\begin{cases}-\sigma_{\max}kT-\dfrac{\delta^2}{4\sigma_{nx}kT}, & T>T_g^{\mathrm{eq}}\\ -(\sigma_{\mathrm{shift}}+\sigma_x)kT-\delta, & T<T_g^{\mathrm{eq}},\end{cases}\tag{A1}$$

$$\frac{S^{\mathrm{eq}}_{nx}}{N}=\frac{3h\nu_0}{T(\xi-1)}-3k\ln\left(1-\frac{1}{\xi}\right)\times\begin{cases}+\sigma_{\max}k-\dfrac{\delta^2}{4\sigma_{nx}kT^2}, & T>T_g^{\mathrm{eq}}\\ +(\sigma_{\mathrm{shift}}+\sigma_x)k, & T<T_g^{\mathrm{eq}},\end{cases}$$

$$\frac{U^{\mathrm{eq}}_{nx}}{N}=\frac{3h\nu_0}{2}+\frac{3h\nu_0}{\xi-1}\begin{cases}-\dfrac{\delta^2}{2\sigma_{nx}kT}, & T>T_g^{\mathrm{eq}}\\ -\delta, & T<T_g^{\mathrm{eq}},\end{cases}$$

$$\frac{C^{\mathrm{eq}}_{nx}}{N}=\frac{3(h\nu_0)^2\xi}{kT^2(\xi-1)^2}\begin{cases}+\dfrac{\delta^2}{2\sigma_{nx}kT^2}, & T>T_g^{\mathrm{eq}}\\ +0, & T<T_g^{\mathrm{eq}},\end{cases}$$

where $\xi=\exp(h\nu_0/kT)$. The value of a^* as a function of temperature, for $\gamma=0$, is

$$\frac{a^*}{N}=\frac{1}{2}-\frac{\delta}{4\sigma_{nx}kT}\left(1+\frac{T_{3/4}}{T}\right),\tag{A2}$$

and so a^* varies more slowly with temperature when σ_{nx} is large and δ is small. The expressions in Eq. (A1) were derived by taking the limit of large N and setting $T_{3/4}$ to zero. They are valid except in the $T\to0$ limit, where terms in $T_{3/4}/T$ can contribute. The correct expression for the configurational entropy for $T<T_g$ is $k(\sigma_{\mathrm{shift}}+\sigma_x)[T(T+2T_{3/4})/(T+T_{3/4})^2]$, and vanishes for $T\to0$ for any large but finite N. The configurational contribution to C^{eq}/N is actually $2k(\sigma_{\mathrm{shift}}+\sigma_x)[TT^2_{3/4}/(T+T_{3/4})^3]$, which has a maximum value of $8k(\sigma_{\mathrm{shift}}+\sigma_x)/27$ at $T=T_{3/4}/2$. If freezing occurs to region a then the corresponding maximum value is $8kN\sigma_a/27$, and again occurs at $T=T_{3/4}/2$. This maximum can just be discerned as a small low-temperature feature in some of the heat capacity plots in Sec. IV; a first-order-like transition occurs within each region.

The analytical result for C^{eq}/N in Eq. (A1) is not accurate near the discontinuity at T_g^{eq}, where the maximum value of $2k\sigma_{nx}$ is an upper limit to the peak in the configurational entropy. However, it still provides a useful measure of the size of the heat capacity feature.

The results in Eq. (A1) can be used to analyze the nature of the underlying equilibrium phase transition in the noncrystalline phase space in the limit of $N\to\infty$. The continuity of the free energy and its first derivative S at T_g^{eq}, and the jump in the heat capacity of $2k\sigma_{nx}$ per atom, indicate a second-order transition according to the Ehrenfest scheme.[132] Gibbs and DiMarzio[48] also obtained a second-order result from their approximate lattice theory for polymer melts, but our result is different because the configurational entropy does not vanish at T_g^{eq}. In fact, Stillinger has previously shown that freezing to a single minimum at finite temperature, as observed in the Gibbs-DiMarzio model,[48] should not occur because the energy density of local minima is likely to be singular at a crystalline or amorphous lower bound.[84] In the present model the system continues to explore an exponentially large number of minima below T_g^{eq}, and the entropy only tends to zero as $T\to0$. This behavior is explicitly built into the model through the form assumed for Z_a^r, and is based upon separate calculations of rearrangement pathways for model glass formers.[32] In these calculations we have found numerous low-energy processes that do not correspond to diffusion, and we therefore expect transitions between local minima to continue below T_g^{eq}. The second-order behavior of the model arises from the change in slope of the entropy as a function of T when the regional occupation probabilities become fixed. The contribution to the entropy from changes in the regional occupations then disappears.

If $T_g = \zeta T_g^{\mathrm{eq}}$, where ζ increases from unity as the observation time scale decreases, we find

$$\frac{\Delta C}{N} = \frac{2k\sigma_{nx}}{\zeta^2} \leqslant 2k\sigma_{nx}, \tag{A3}$$

where ΔC is the step in the heat capacity at T_g under the same conditions as for Eq. (A1). The glass transition is therefore accompanied by a larger heat-capacity peak and change in slope of the entropy when the number of noncrystalline minima is larger, as anticipated by Angell.[95] These features are also larger the closer T_g is to T_g^{eq}, as expected, and can clearly be seen in the results presented in Sec. IV.

A simple analytical expression for the relaxation time t can also be obtained using a^*. For $\gamma = 0$ we find

$$\ln t = \frac{1}{kT}\left(\Delta A_{\max} - \frac{h\nu_0}{2} + \delta - (\Delta A_{\max} - \Delta A_{\min}) \times \left[\frac{1}{2}\left(1 - \frac{T_g^{\mathrm{eq}}}{T} \right) \right]^{\alpha} \right) + \ln \frac{h}{kT(1-1/\xi)}, \tag{A4}$$

where $\xi = \exp(h\nu_0/kT)$, as above. The above expression is accurate so long as the value of a corresponding to the largest contribution to the flux is not too different from a^*, which corresponds to the maximum term in the partition function. In practice, Eq. (A4) loses accuracy as the system approaches T_g, but is still useful for understanding the trends observed. For high temperature,

$$\ln t = -\ln \nu_0 + \left(\frac{1}{kT} \right)(\Delta A_{\min} + \delta) + \left(\frac{1}{kT} \right)^2 \left(\frac{\alpha\delta(\Delta A_{\max} - \Delta A_{\min})}{2\sigma_{nx}} - \frac{h^2\nu_0^2}{24} \right) + \left(\frac{1}{kT} \right)^3 \frac{(1-\alpha)\alpha(\Delta A_{\max} - \Delta A_{\min})\delta^2}{8\sigma_{nx}^2} + \cdots . \tag{A5}$$

Equation (A5) shows that the t plots should have intercept $-\log_{10}\nu_0$ and initial slope $(\Delta A_{\min} + \delta) T_g \log_{10} e/k$.

[1] W. Götze, in *Liquids, Freezing and the Glass Transition*, Les Houches, Session LI, 1989, edited by J.-P. Hansen, D. Levesque, and J. Zinn-Justin (North-Holland, Amsterdam, 1991), pp. 287–499.
[2] W. Kob, ACS Symp. Ser. **676**, 28 (1997).
[3] W. Götze, J. Phys.: Condens. Matter **11**, A1 (1999).
[4] D. J. Wales, J. P. K. Doye, M. A. Miller, P. N. Mortenson, and T. R. Walsh, Adv. Chem. Phys. **115**, 1 (2000).
[5] F. H. Stillinger and T. A. Weber, Phys. Rev. A **25**, 978 (1982).
[6] F. H. Stillinger and T. A. Weber, J. Phys. Chem. **87**, 2833 (1983).
[7] F. H. Stillinger and T. A. Weber, J. Chem. Phys. **80**, 2742 (1984).
[8] F. H. Stillinger, Phys. Rev. E **59**, 48 (1999).
[9] R. S. Berry and R. Breitengraser-Kunz, Phys. Rev. Lett. **74**, 3951 (1995).
[10] R. E. Kunz and R. S. Berry, J. Chem. Phys. **103**, 1904 (1995).
[11] B. Kunz, R. S. Berry, and T. Astakhova, Surf. Rev. Lett. **3**, 307 (1996).
[12] R. E. Kunz, P. Blaudeck, K. H. Hoffmann, and R. S. Berry, J. Chem. Phys. **108**, 2576 (1998).
[13] J. P. K. Doye and D. J. Wales, J. Chem. Phys. **105**, 8428 (1996).
[14] O. M. Becker and M. Karplus, J. Chem. Phys. **106**, 1495 (1997).
[15] A. Heuer, Phys. Rev. Lett. **78**, 4051 (1997).
[16] T. R. Walsh and D. J. Wales, J. Chem. Phys. **109**, 6691 (1998).
[17] M. Cieplak, M. Henkel, J. Karbowski, and J. R. Banavar, Phys. Rev. Lett. **80**, 3654 (1998).
[18] L. Angelani, G. Parisi, G. Ruocco, and G. Viliani, Phys. Rev. Lett. **81**, 4648 (1998).
[19] K. D. Ball and R. S. Berry, J. Chem. Phys. **109**, 8541 (1998).
[20] K. D. Ball and R. S. Berry, J. Chem. Phys. **109**, 8557 (1998).
[21] M. A. Miller and D. J. Wales, J. Chem. Phys. **111**, 6610 (1999).
[22] M. A. Miller, J. P. K. Doye, and D. J. Wales, J. Chem. Phys. **110**, 328 (1999).
[23] J. P. K. Doye and D. J. Wales, Phys. Rev. B **59**, 2292 (1999).
[24] M. A. Miller, J. P. K. Doye, and D. J. Wales, Phys. Rev. E **60**, 3701 (1999).
[25] J. P. K. Doye and D. J. Wales, J. Chem. Phys. **111**, 11 070 (1999).
[26] S. Büchner and A. Heuer, Phys. Rev. E **60**, 6507 (1999).
[27] F. Sciortino, W. Kob, and P. Tartaglia, Phys. Rev. Lett. **83**, 3214 (1999).
[28] K. M. Westerberg and C. A. Floudas, J. Global Optim. **15**, 261 (1999).
[29] K. D. Ball and R. S. Berry, J. Chem. Phys. **111**, 2060 (1999).
[30] L. Angelani, G. Parisi, G. Ruocco, and G. Viliani, Phys. Rev. E **61**, 1681 (2000).
[31] N. Mousseau, cond-mat/004356 (unpublished).
[32] T. F. Middleton and D. J. Wales, Phys. Rev. B (to be published).
[33] L. Angelani, R. Di Leonardo, G. Ruocco, A. Scala, and F. Sciortino, Phys. Rev. Lett. **85**, 5356 (2000).
[34] K. Broderix, K. K. Bhattacharya, A. Cavagna, A. Zippelius, and I. Giardina, Phys. Rev. Lett. **85**, 5360 (2000).
[35] H. Frauenfelder, S. G. Sligar, and P. G. Wolynes, Science **254**, 1598 (1991).
[36] P. Leopold, M. Montal, and J. Onuchic, Proc. Natl. Acad. Sci. U.S.A. **89**, 8721 (1992).
[37] J. D. Bryngelson, J. N. Onuchic, N. D. Socci, and P. G. Wolynes, Proteins **21**, 167 (1995).
[38] P. G. Wolynes, J. N. Onuchic, and D. Thirumalai, J. Chem. Phys. **102**, 1619 (1995).
[39] N. D. Socci, J. N. Onuchic, and P. G. Wolynes, Proteins: Struct., Funct., Genet. **32**, 136 (1998).
[40] J. G. Saven, J. Wang, and P. G. Wolynes, J. Chem. Phys. **101**, 11 037 (1994).

[41] V. I. Abkevich, A. M. Gutin, and E. I. Shakhnovich, J. Chem. Phys. **101**, 6052 (1994).
[42] J. Wang, J. N. Onuchic, and P. G. Wolynes, Phys. Rev. Lett. **76**, 4861 (1996).
[43] J. Wang, J. G. Saven, and P. G. Wolynes, J. Chem. Phys. **105**, 11 276 (1996).
[44] A. Gutin, A. Sali, V. Abkevich, M. Karplus, and E. I. Shakhnovich, J. Chem. Phys. **108**, 6466 (1998).
[45] M. Goldstein, J. Chem. Phys. **51**, 3728 (1969).
[46] G. P. Johari and M. Goldstein, J. Chem. Phys. **53**, 2372 (1970).
[47] G. Adam and J. H. Gibbs, J. Chem. Phys. **43**, 139 (1965).
[48] J. H. Gibbs and E. A. DiMarzio, J. Chem. Phys. **28**, 373 (1958).
[49] K. L. Ngai, J. Phys. Chem. B **103**, 5895 (1999).
[50] X. P. Tang, U. Geyer, R. Busch, W. L. Johnson, and Y. Wu, Nature (London) **402**, 160 (1999).
[51] A. Scala, F. W. Starr, E. La Nave, F. Sciortino, and H. E. Stanley, Nature (London) **406**, 166 (2000).
[52] S. Sastry, Nature (London) **409**, 164 (2001).
[53] S. Sastry, Phys. Rev. Lett. **85**, 590 (2000).
[54] X. Y. Xia and P. G. Wolynes, Proc. Natl. Acad. Sci. U.S.A. **97**, 2990 (2000).
[55] N. Agmon and J. J. Hopfield, J. Chem. Phys. **78**, 6947 (1983).
[56] D. Beece, L. Eisenstein, H. Frauenfelder, D. Good, M. C. Marden, L. Reinisch, A. H. Reynolds, L. B. Sorensen, and K. T. Yue, Biochemistry **19**, 5147 (1980).
[57] S. A. Brawer, J. Chem. Phys. **81**, 954 (1984).
[58] M. Goldstein, Faraday Symp. Chem. Soc. **6**, 7 (1972).
[59] E. Donth, J. Non-Cryst. Solids **53**, 325 (1982).
[60] D. L. Stein and R. G. Palmer, Phys. Rev. B **38**, 12 035 (1988).
[61] D. Kivelson, S. A. Kivelson, X. Zhao, and G. Tarjus, Physica A **219**, 27 (1995).
[62] J. C. Dyre, Phys. Rev. Lett. **58**, 792 (1987).
[63] H. Tanaka, J. Chem. Phys. **111**, 3163 (1999).
[64] H. Tanaka, J. Chem. Phys. **111**, 3175 (1999).
[65] H. Bässler, Phys. Rev. Lett. **58**, 767 (1987).
[66] V. I. Arkhipov and H. Bässler, J. Phys. Chem. **98**, 662 (1994).
[67] J. C. Dyre, Phys. Rev. B **51**, 12 276 (1995).
[68] G. Diezemann, J. Chem. Phys. **107**, 10 112 (1997).
[69] G. Diezemann, H. Sillescu, G. Hinze, and R. Bohmer, Phys. Rev. E **57**, 4398 (1998).
[70] G. Diezemann and K. Nelson, J. Phys. Chem. B **103**, 4089 (1999).
[71] R. G. Palmer, Adv. Phys. **31**, 669 (1982).
[72] R. Zwanzig, J. Chem. Phys. **103**, 9397 (1995).
[73] K. H. Fischer and J. A. Hertz, *Spin Glasses* (Cambridge University Press, Cambridge, 1991).
[74] T. R. Kirkpatrick and P. G. Wolynes, Phys. Rev. B **36**, 8552 (1987).
[75] T. R. Kirkpatrick and P. G. Wolynes, Phys. Rev. A **35**, 3072 (1987).
[76] T. R. Kirkpatrick, D. Thirumalai, and P. G. Wolynes, Phys. Rev. A **40**, 1045 (1989).
[77] M. Dzugutov, J. Phys.: Condens. Matter **11**, A253 (1999).
[78] R. J. Speedy, J. Mol. Struct. **485-486**, 537 (1999).
[79] S. K. Ma, *Statistical Mechanics* (World Scientific, Singapore, 1985).
[80] C. T. Moynihan, A. J. Easteal, and J. Wilder, J. Phys. Chem. **78**, 2673 (1974).
[81] D. J. McGinty, J. Chem. Phys. **55**, 580 (1971).
[82] J. J. Burton, J. Chem. Phys. **56**, 3133 (1972).
[83] M. R. Hoare, Adv. Chem. Phys. **40**, 49 (1979).
[84] F. H. Stillinger, J. Chem. Phys. **88**, 7818 (1988).
[85] G. Franke, E. R. Hilf, and P. Borrmann, J. Chem. Phys. **98**, 3496 (1993).
[86] D. J. Wales, Mol. Phys. **78**, 151 (1993).
[87] C. J. Tsai and K. D. Jordan, J. Phys. Chem. **97**, 11 227 (1993).
[88] G. P. Johari, J. Chem. Phys. **112**, 7518 (2000).
[89] D. J. Wales, Chem. Phys. Lett. **285**, 330 (1998).
[90] D. J. Wales, Chem. Phys. Lett. **294**, 262 (1998).
[91] A. Heuer and S. Büchner, J. Phys.: Condens. Matter **12**, 6535 (2000).
[92] F. H. Stillinger and T. A. Weber, Phys. Rev. B **31**, 5262 (1985).
[93] P. C. Haarhoff, Mol. Phys. **7**, 101 (1963).
[94] J. P. K. Doye and D. J. Wales, J. Chem. Phys. **102**, 9659 (1995).
[95] C. A. Angell, Science **267**, 1924 (1995).
[96] G. P. Johari, Philos. Mag. **41**, 41 (1981).
[97] A. P. Sokolov, A. Kisliuk, M. Soltwisch, and D. Quitmann, Phys. Rev. Lett. **69**, 1540 (1992).
[98] C. A. Angell, J. Phys.: Condens. Matter **12**, 6463 (2000).
[99] D. Wales, M. Miller, and T. Walsh, Nature (London) **394**, 758 (1998).
[100] N. G. van Kampen, *Stochastic Processes in Physics and Chemistry* (North-Holland, Amsterdam, 1981).
[101] R. E. Kunz, *Dynamics of First-Order Phase Transitions* (Deutsch, Thun, 1995).
[102] R. G. Palmer, D. L. Stein, E. Abrahams, and P. W. Anderson, Phys. Rev. Lett. **53**, 958 (1984).
[103] B. A. Huberman and M. Kerszberg, J. Phys. A **18**, L331 (1985).
[104] J. Sabelko, J. Ervin, and M. Gruebele, Proc. Natl. Acad. Sci. U.S.A. **96**, 6031 (1999).
[105] C. A. Angell, Prog. Theor. Phys. Suppl. **126**, 1 (1997).
[106] J. L. Green, K. Ito, K. Xu, and C. A. Angell, J. Phys. Chem. B **103**, 3991 (1999).
[107] G. Fulcher, J. Am. Ceram. Soc. **8**, 339 (1925).
[108] H. Vogel, Z. Phys. **22**, 645 (1921).
[109] G. Tammann and W. Hesse, Z. Anorg. Allg. Chem. **156**, 245 (1926).
[110] J. D. Ferry, L. D. Grandine, and E. R. Fitzgerald, J. Appl. Phys. **24**, 911 (1953).
[111] W. Kauzmann, Chem. Rev. **43**, 219 (1948).
[112] K. Ito, C. T. Moynihan, and C. A. Angell, Nature (London) **398**, 492 (1999).
[113] G. Tarjus, D. Kivelson, and P. Viot, J. Phys.: Condens. Matter **12**, 6497 (2000).
[114] R. K. Bowles and R. J. Speedy, Mol. Phys. **87**, 1349 (1996).
[115] K. W. Wojciechowski, D. Frenkel, and A. C. Branka, Phys. Rev. Lett. **66**, 3168 (1991).
[116] K. W. Wojciechowski, A. C. Branka, and D. Frenkel, Physica A **196**, 519 (1993).
[117] E. D. Eastman and R. T. Milner, J. Chem. Phys. **1**, 444 (1933).
[118] F. Simon, Physica (Amsterdam) **IV**, 1089 (1937).
[119] R. H. Fowler and E. A. Guggenheim, *Statistical Thermodynamics*, 3rd ed. (Cambridge University Press, Cambridge, 1952).
[120] M. S. Westwell, M. S. Searle, D. J. Wales, and D. H. Williams, J. Am. Chem. Soc. **117**, 5013 (1995).
[121] F. H. Stillinger and T. A. Weber, Phys. Rev. A **28**, 2408 (1983).
[122] M. Dzugutov, Nature (London) **381**, 137 (1996).

[123] S. Sastry, P. G. Debenedetti, and F. H. Stillinger, Nature (London) **393**, 554 (1998).
[124] H. Jonsson and H. C. Andersen, Phys. Rev. Lett. **60**, 2295 (1988).
[125] P. Jund and R. Jullien, Phys. Rev. Lett. **83**, 2210 (1999).
[126] T. B. Schroder, S. Sastry, J. C. Dyre, and S. C. Glotzer, J. Chem. Phys. **112**, 9834 (2000).
[127] D. J. Lacks, Phys. Rev. Lett. **80**, 5385 (1998).
[128] D. L. Malandro and D. J. Lacks, J. Chem. Phys. **107**, 5804 (1997).
[129] T. M. Nieuwenhuizen, Phys. Rev. Lett. **78**, 3491 (1997).
[130] D. C. Wallace, Phys. Rev. E **60**, 7049 (1999).
[131] M. Mezard and G. Parisi, J. Chem. Phys. **111**, 1076 (1999).
[132] P. Ehrenfest, in *Collected Scientific Papers*, edited by M. J. Klein (North-Holland, Amsterdam, 1959).